

Astronomy & Astrophysics manuscript no.  
 (will be inserted by hand later)

# H $\alpha$ surface photometry of galaxies in the Virgo cluster. IV: the current star formation in nearby clusters of galaxies \*

G. Gavazzi<sup>1</sup>, A. Boselli<sup>2</sup>, P. Pedotti<sup>1</sup>, A. Gallazzi<sup>1</sup>, and L. Carrasco<sup>3,4</sup>

<sup>1</sup> Università degli Studi di Milano-Bicocca, Piazza delle scienze 3, 20126 Milano, Italy  
 e-mail: giuseppe.gavazzi@mib.infn.it

<sup>2</sup> Laboratoire d'Astrophysique de Marseille, Traverse du Siphon, F-13376 Marseille Cedex 12, France  
 e-mail: Alessandro.Boselli@astrsp-mrs.fr

<sup>3</sup> Instituto Nacional de Astrofísica, Óptica y Electrónica, Apartado Postal 51. C.P. 72000 Puebla, Pue., México  
 e-mail: carrasco@transun.inaoep.mx

<sup>4</sup> Observatorio Astronómico Nacional, UNAM, Apartado Postal 877, C.P. 22860, Ensenada B.C., México

**Abstract.** H $\alpha$ +[NII] imaging observations of 369 late-type (spiral) galaxies in the Virgo cluster and in the Coma/A1367 supercluster are analyzed, covering 3 rich nearby clusters (A1367, Coma and Virgo) and nearly isolated galaxies in the Great-Wall. They constitute an optically selected sample ( $m_p < 16.0$ ) observed with  $\sim 60\%$  completeness. These observations provide us with the current ( $T < 10^7$  yrs) star formation properties of galaxies that we study as a function of the clustercentric projected distances ( $\Theta$ ). The expected decrease of the star formation rate (SFR), as traced by the H $\alpha$  E.W., with decreasing  $\Theta$  is found only when galaxies brighter than  $M_p \sim -19.5$  are considered. Fainter objects show no or reverse trends. We also include in our analysis Near Infrared data, providing us with informations on the old ( $T > 10^9$  yrs) stars. Put together, the young and the old stellar indicators give the ratio of currently formed stars over the stars formed in the past, or "birthrate" parameter  $b$ . For the considered galaxies we also determine the "global gas content" combining HI with CO observations. We define the "gas deficiency" parameter as the logarithmic difference between the gas content of isolated galaxies of a given Hubble type and the measured gas content. For the isolated objects we find that  $b$  decreases with increasing NIR luminosity. In other words less massive galaxies are currently forming stars at higher rate than their giant counterparts which experienced most of their star formation activity at earlier cosmological epochs. The gas-deficient objects, primarily members to the Virgo cluster, have their birthrate significantly lower than the isolated objects with normal gas content and of similar NIR luminosity. This indicates that the current star formation is regulated by the gaseous content of spirals. Whatever mechanism (most plausibly ram-pressure stripping) is responsible for the pattern of gas deficiency observed in spiral galaxies members to rich clusters, it also produces the observed quenching of the current star formation. A significant fraction of gas "healthy" (i.e. with a gas deficiency parameter less than 0.4) and currently star forming galaxies is unexpectedly found projected near the center of the Virgo cluster. Their average Tully-Fisher distance is found approximately one magnitude further away ( $\mu_o = 31.77$ ) than the distance of their gas-deficient counterparts ( $\mu_o = 30.85$ ), suggesting that the gas healthy objects belong to a cloud projected onto the cluster center, but in fact lying few Mpc behind Virgo, thus unaffected by the dense IGM of the cluster.

**Key words.** Galaxies: Galaxies: photometry; Galaxies: clusters: individual: Virgo

## 1. Introduction

A significant trend of the global star formation rate (SFR) of galaxies with the projected clustercentric distance from rich clusters of galaxies is well documented in the local universe ( $0.05 < z < 0.1$ ). The mean SFR, as traced by the equivalent width of the H $\alpha$  line (Kennicutt 1989), is

Send offprint requests to: G. Gavazzi

\* based on observations taken at the Observatorio Astronómico Nacional (Mexico), the OHP (France), Calar Alto and NOT (Spain) observatories.

found to decrease with decreasing distance from rich clusters (Lewis et al. 2002). This pattern is dominated by the "morphology segregation" effect (Dressler 1980), i.e. elliptical and spheroidal galaxies with little or no current star formation overcome in number the star forming galaxies in the center of rich clusters. What physical mechanism (nature vs. nurture) is responsible for the morphological transformation taking place in the densest environments is however not yet fully understood. To shed light on the various possibilities, i.e. galaxy harassment (Moore et al., 1996, 1998), tidal stirring (Mayer et al. 2001) or ram pres-

sure stripping (Gunn & Gott 1972), it is crucial to establish observationally if, beside the morphology segregation, galaxies of a given morphological type, namely the spirals, are affected by a systematic SFR decrease toward the center of nearby clusters.

If on one hand Kennicutt (1983) found that spirals in the Virgo cluster have their mean SFR as much as a factor of two lower than isolated galaxies, Gavazzi et al. (1998) did not confirm this evidence in the Coma and A1367 clusters. Moreover Iglesias-Paramo et al. (2002) found that the shape of the H $\alpha$  luminosity function of these two clusters does not differ significantly from the one of isolated galaxies. The result of Kennicutt (1983) was based on only a dozen giant galaxies with H $\alpha$  measurements from aperture photometry, thus requiring a confirmation on a larger sample with modern imaging data.

With the aim of solving this riddle we undertook an H $\alpha$  imaging survey of two optically complete samples of galaxies. The first is composed of nearly isolated objects selected from the CGCG (Zwicky et al. 1961-68) in the bridge between Coma and A1367, which we observed down to the limit of 15.7 mag. This constitutes our reference sample of non-cluster objects. The cluster sample is focused on A1367, the Coma and the Virgo clusters. We took H $\alpha$  imaging observations of these regions (Gavazzi et al. 1998, Gavazzi et al. 2002a, Paper I of this series; Boselli & Gavazzi 2002; paper II and Boselli et al. 2002b; paper III). Our own observations were complemented with data taken from the literature (Kennicutt & Kent 1983, Romanishin 1990, Gavazzi et al. 1991, Young et al. 1996; Koopmann et al. 2001).

Furthermore we performed a NIR imaging survey of the same regions (Gavazzi et al. 2000b and references therein), providing informations on the old stars.

In the present paper we combine H $\alpha$  with NIR measurements to study the young and the old components of the stellar population integrated over the whole galaxies and we analyze the properties of the stars as a function of the clustercentric projected distance, of the luminosity and of the global gas content. We postpone to a forthcoming paper the morphological aspects of the analysis related to the spatial distribution of the young/old stars. The present paper is organized as follows: in Section 2 we briefly present the new H $\alpha$  imaging observations of 13 galaxies. The sample used in the present investigation is illustrated in Section 3. After defining the "birth-rate" parameter (Sect. 4.1) and the "gas-deficiency" parameter (Sect. 4.2), we analyze in Section 5.1 the clustercentric dependence of the current star formation rate. In Sections 5.2 and 5.3 we study the current star formation properties of galaxies in 3 local clusters as a function of their global luminosity and gaseous properties. The conclusions are briefly discussed in Section 6 and summarized in Section 7.

## 2. New observations

Narrow band imaging in the H $\alpha$  emission line ( $\lambda = 6562.8$  Å) of 13 galaxies was obtained in march 20, 2002, using the 2.1m telescope at San Pedro Martir Observatory (SPM) (Baja California, Mexico).

The target galaxies are listed in Table 3 as follows:

- Column 1: VCC (Binggeli et al. 1985) or CGCG (Zwicky et al. 1961-68) designation.
- Column 2: NGC/IC name.
- Column 3: UGC name.
- Columns 4 and 5: J2000 celestial coordinates.
- Column 6: photographic magnitude as given in the VCC or in the CGCG.
- Column 7: heliocentric velocity (km s $^{-1}$ ) from the VCC or from Gavazzi et al. (1999a).
- Column 8: exposure times in minutes for the ON-band filter.
- Column 9: transmissivity ( $R_{ON}$ ) of the ON-band filter at the redshifted H $\alpha$  line.

We used a Site 1024×1024 pixels CCD detector with pixel size of 0.31 arcsec. Each galaxy was observed through a narrow band interferometric filter ( $\sim 90$  Å width) centered at  $\lambda 6603$ , for the galaxies at the redshift of Virgo ( $350 < V < 3000$  km sec $^{-1}$ ), and at  $\lambda 6723$  Å, for galaxies in the Coma supercluster. These observations provided us with the ON-band images and required 15-20 min integration time. The OFF-band images were obtained through the r-Gunn filter and were exposed one fifth of the ON-band ones. The observations were obtained with the seeing ranging from 1.2 to 3 arcsec, but in photometric conditions. They were flux calibrated using the standard stars Feige 34 and Hz44 from the catalogue of Massey et al. (1988), observed every 2 hours. Repeated measurements gave  $< 0.05$  mag differences, which we assume as the typical uncertainty ( $1\sigma$ ) of the photometric results given in this work.

The reduction of the CCD frames follows a procedure identical to the one described in previous papers of this series (e.g. Gavazzi et al. 2002), based on the IRAF STSDAS<sup>1</sup> reduction packages, and it will be briefly summarized here. To remove the detector response each image was bias subtracted and divided by the median of several flat field exposures obtained on empty regions of the twilight sky. Cosmic rays were removed either using the task COSMICRAY in IRAF or manually by direct inspection of the frames. The sky background was determined in each frame in concentric object-free regions around the galaxies and then subtracted from the flat-fielded images. The

<sup>1</sup> IRAF is the Image Analysis and Reduction Facility made available to the astronomical community by the National Optical Astronomy Observatories, which are operated by AURA, Inc., under contract with the U.S. National Science Foundation. STSDAS is distributed by the Space Telescope Science Institute, which is operated by the Association of Universities for Research in Astronomy (AURA), Inc., under NASA contract NAS 5-26555.

typical uncertainty on the mean background is estimated 10 % of the rms in the individual pixels. This represents the dominant source of error in low S/N regions.

H $\alpha$  Fluxes and equivalent widths are estimated subtracting the contribution of the continuum from the ON-band measurements. As the continuum was estimated using the broad band  $r$  filter, which in fact includes the H $\alpha$  and [NII] lines, the corrected fluxes and equivalent widths are computed according to eq. (1) and (2) of paper III, and their uncertainties are given by:

$$\sigma_{F_c} = \sigma_F \left( 1 + \frac{\int R_{ON}(\lambda) d\lambda}{\int R_{OFF}(\lambda) d\lambda} \right) \quad (1)$$

$$\begin{aligned} \sigma_{E.W.c} = \sigma_{E.W.} & \left( 1 + \frac{\int R_{ON}(\lambda) d\lambda}{\int R_{OFF}(\lambda) d\lambda} \right) \\ & \times \left( \frac{1}{1 - (\frac{E.W.}{\int R_{OFF}(\lambda) d\lambda})^2} \right) \end{aligned} \quad (2)$$

Galaxies with substantial H $\alpha$  + [NII] structure are given in Fig.14. The contours of the OFF frames are superposed to the NET (ON-OFF) frames (grey-scale).

### 3. The sample

Including the new observations presented in this paper, this work comprises H $\alpha$  and NIR (H band) imaging observations of 369 late-type galaxies belonging to the Virgo cluster and to the Coma supercluster region.

The Virgo cluster galaxies were selected from the Virgo Cluster Catalogue (VCC) of Binggeli et al. (1985), with  $m_p \leq 16.0$ , Hubble type later than S0a (as given in the VCC) and classified as cluster members, possible members or belonging to the W, W', M clouds or to the southern extension (Binggeli et al. 1985; 1993; see also Gavazzi et al. 1999a) matching  $V < 3000$  km s $^{-1}$  (see Fig. 1).

The late-type ( $> S0a$ ) galaxies in the Coma supercluster region ( $18^\circ \leq \delta \leq 32^\circ$ ;  $11.5^\text{h} \leq \alpha \leq 13.5^\text{h}$ ) were selected from the CGCG catalogue ( $m_p \leq 15.7$ ) (Zwicky et al. 1961-68) and include members to the Coma Supercluster according to Gavazzi et al. (1999b) (see Fig. 2). Table 1 gives the details of the sample completeness in the two studied regions. The Coma supercluster members are divided in cluster (A1367+A1656) members, members to groups and pairs (see Gavazzi et al. 1999b) and strictly isolated supercluster objects (with projected separations  $> 300$  kpc). The H $\alpha$  observations were taken either from the present series of papers (Paper I, II, III, IV, primarily devoted to the Virgo cluster), from Gavazzi et al. (1991, 1998) (containing mostly observations of the Coma supercluster region) or from Kennicutt & Kent (1983), Kennicutt, Bothun & Schommer (1984), Romanishin (1990), Koopmann et al. (2001) (see detailed references in Table 4).

The NIR observations were taken from the series of papers "Near-infrared H surface photometry of galaxies"

(Gavazzi et al. 1996a, b, 2000a, Boselli et al. 1997; Boselli et al. 2000 and from Gavazzi et al. 2001). Total asymptotic H band magnitudes were obtained by Gavazzi et al. (2000b) and by Gavazzi et al. (2001).

As listed in Table 1 the combined NIR+ H $\alpha$  observations cover more than 60 % of the targets in all regions (except Coma supercluster groups+pairs), thus our data can be considered as representative of the late-type galaxies in the studied regions.

The analyzed galaxies are listed in Table 4 as follows:<sup>2</sup>

- Column 1: VCC designation, from Binggeli et al. (1985) for Virgo galaxies, or CGCG (Zwicky et al. 1961-68) for Coma supercluster galaxies.
- Column 2: the membership to a cluster or supercluster, defined as in Gavazzi et al. (1999a) for Virgo and Gavazzi et al. (1999b) for the Coma/A1367 supercluster
- Column 3: morphological type as given in the VCC or in Gavazzi & Boselli (1996).
- Column 4: projected angular separation from the nearest cluster center (degrees).
- Column 5: asymptotic H band magnitude, obtained as described in Gavazzi et al. (2000b).
- Column 6: distance (Mpc); we assume 17 Mpc for Virgo A, N, S, E, 23 Mpc for Virgo B and 32 Mpc for Virgo W, M as given in Gavazzi et al. (1999a), 96 Mpc for Coma, 91 Mpc for A1367. For galaxies not belonging to the clusters, the distance is determined from the redshift using  $H_0 = 75$  km s $^{-1}$ Mpc $^{-1}$ .
- Column 7: gas deficiency parameter as defined in Section 4.2.
- Column 8: H $\alpha$  + [NII]E.W.(Å).
- Column 9: Log of the H $\alpha$  flux (erg cm $^{-2}$  s $^{-1}$ ) de-blended from the [NII] contribution and corrected for internal extinction as in Boselli et al. (2001).
- Column 10: reference to the H $\alpha$  data (as listed at the bottom of the Table).

### 4. Tools

#### 4.1. The birthrate parameter

H $\alpha$  and NIR observations provide us with information on stellar populations with different time scales:  $\sim 10^7$  yrs the former and  $\sim 10^{10}$  yrs the latter. The two quantities combined give the ratio of the current SFR to the average past SFR or the birthrate parameter  $b$ , as defined by Kennicutt et al. (1994).

Following Boselli et al. (2001), we use the Near Infrared luminosity  $L_H$  as a tracer of the global mass of old stars, assuming that disk galaxies have a constant  $M_{Tot}/L_H = 4.6$

<sup>2</sup> Table 4 is only available in electronic form at <http://www.edpsciences.org>

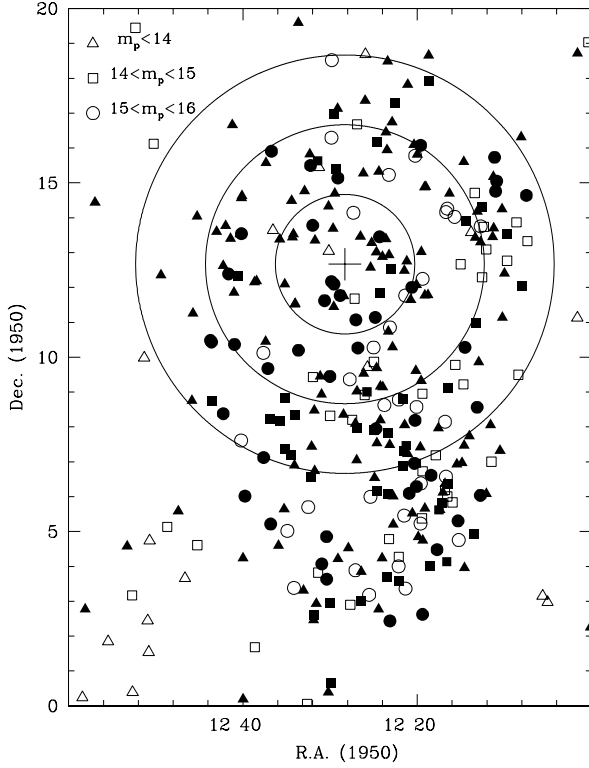


**Fig. 1.** Sky distribution of the 312 spiral galaxies brighter than  $m_p \leq 16.0$  in the VCC. The filled symbols represent 235 galaxies with available H $\alpha$  data, the empty ones to unobserved galaxies. Circles are drawn at 2, 4, 6 deg. projected radial distance from M87 (cross).

**Table 1.** The sample completeness

region	$m_p \leq 16.0$	with NIR	with NIR & H $\alpha$	Compl.
Virgo	323	271	205	63%
ComaS. (Clusters)	72	72	54	75%
ComaS. (Grps + Prs)	67	67	27	40%
ComaS. (Isolated)	119	83	83	69%
Tot.	568	480	356	63%

within their optical radius (Gavazzi et al. 1996c). Thus we write the adimensional parameter  $b$  as:

$$b_{obs} = \frac{SFR t_o (1 - R)}{L_H (M_{Tot}/L_H) DM_{cont}} \quad (3)$$

where SFR is derived from the H $\alpha$  luminosity with:

$$SFR[M \odot yr^{-1}] = K_{H\alpha} L_{H\alpha}[erg s^{-1}] \quad (4)$$

Obviously the H $\alpha$  luminosity is deblended from the observed [NII] contribution and corrected for internal extinction as in Boselli et al. (2001). For consistency with Boselli et al. (2001) we adopt  $K_{H\alpha} = 1/1.16 10^{41}$  for an IMF of slope -2.5 in the mass range 0.1–80  $M\odot$ .

$DM_{cont}$  is the dark matter contribution at the optical radius, i.e. within the 25 mag arcsec $^{-2}$  B band isophote,

that we assume  $DM_{cont}=0.5$ , as in Kennicutt et al. (1994).  $R = 0.3$  (Kennicutt et al. 1994) is the fraction of gas that stars re-injected through stellar winds into the interstellar medium during their lifetime, that we assume  $t_o \sim 12$  Gyrs.

If we assume that galaxies evolved as "closed" systems following an exponential Star Formation History (SFH), with a characteristic decay time  $\tau$  since their epoch of formation ( $t_o$ ), their birthrate parameter can be computed analytically (see Boselli et al. 2001) as:

$$b_{mod} = \frac{t_o e^{-t_o/\tau}}{\tau(1 - e^{-t_o/\tau})} \quad (5)$$

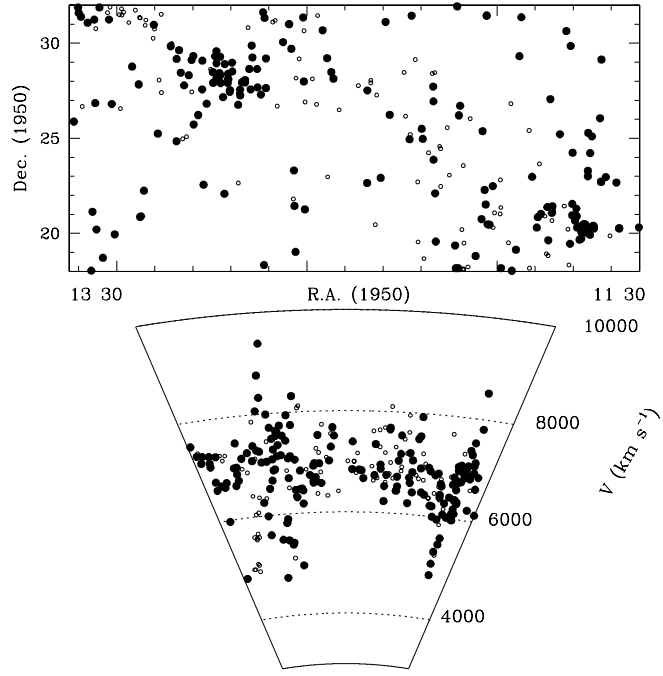


**Fig. 2.** Sky distribution of the 256 spiral galaxies brighter than  $m_p \leq 15.7$  in the CGCG in the Coma supercluster region (top). Wedge diagram (bottom). The filled symbols represent 158 galaxies with available H $\alpha$  data, the empty ones to unobserved galaxies.

$b_{mod}$  can be written as a function of  $L_H$  using the relation between  $\tau$  and  $L_H$  found by Boselli et al. (2001):

$$\log \tau = -0.4(\log L_H - 12)[\text{Gyr}] \quad (6)$$

where

$$\log L_H = 11.36 - 0.4H + 2\log(\text{Dist})[\text{L}_H \odot] \quad (7)$$

The dependence of  $b_{mod}$  on  $L_H$  is given as a dotted line in Figs. 8, 9 and 10.

Although  $b$  and  $H_\alpha$  E.W. have distinct dimensions, they are strongly correlated quantities. In fact they are operationally obtained in a similar way:  $b$  is computed by normalizing the  $H_\alpha$  line intensity to the NIR continuum intensity, while the equivalent width is divided by the continuum intensity underlying the  $H_\alpha$  line. This is shown in Fig. 3 which can be directly compared with Fig. 4 of Kennicutt et al. (1994).

#### 4.2. The global gas deficiency parameter

For galaxies in our sample we estimate the "global gas content"  $M_{gas} = M_{HI} + M_{H2} + M_{He}$ .

$M_{HI}$  is available for most (95 %) targets by direct 21 cm observations (see Scudiego & Gavazzi 1993, Hoffman et al. 1996, and references therein). The mass of molecular hydrogen can be estimated from the measurement of the

CO (1-0) line emission, assuming a conversion factor ( $X$ ) between this quantity and the  $H_2$  surface density.  $X$  is known to vary in the range  $10^{20}$  to  $10^{21}$  [mol cm $^{-2}$  (K km s $^{-1}$ ) $^{-1}$ ] from galaxy to galaxy, according to their metallicity and UV radiation field. We adopt the empirical calibration as a function of the H band luminosity:

$$\log X = 24.23 - 0.38 * \log L_H \quad (8)$$

found by Boselli et al. (2002a). The CO (1-0) line emission is unfortunately available for 52 % of the considered sample (see Boselli et al. 2002a and references therein), and it is assumed 15 % of the HI content for the remaining objects (as concluded by Boselli et al. 2002a).

The contribution of He, not directly observable, is estimated as 30 % of  $M_{HI} + M_{H2}$  (see Boselli et al. 2002a). We define the "gas deficiency" parameter  $Def_{gas} = \log M_{gas\ ref.} - \log M_{gas\ obs.}$  as the logarithmic difference between  $M_{gas}$  of a reference sample of isolated galaxies and  $M_{gas}$  actually observed in individual objects (in full analogy with the definition of HI deficiency by Giovanelli & Haynes 1985). Using a procedure similar to the one adopted by Haynes and Giovanelli (1984) we find that the gas content of 72 isolated objects in the Coma Supercluster correlates with their linear optical diameter ( $D$ ):  $\log M_{gas\ ref.} = a + b \log(D)$ , where  $a$  and  $b$  are weak functions of the Hubble type, as listed in Table 2.  $Def_{gas}$  are listed in Column 7 of Table 4. Histograms of

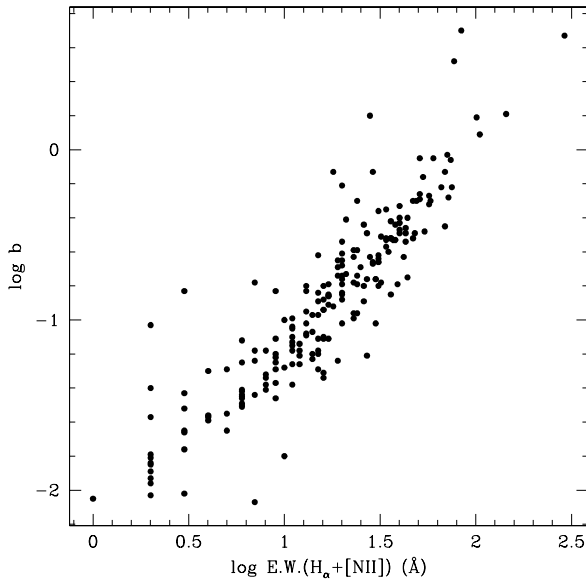


**Fig. 3.** The relation between the birthrate parameter and the H $\alpha$  emission line equivalent width.

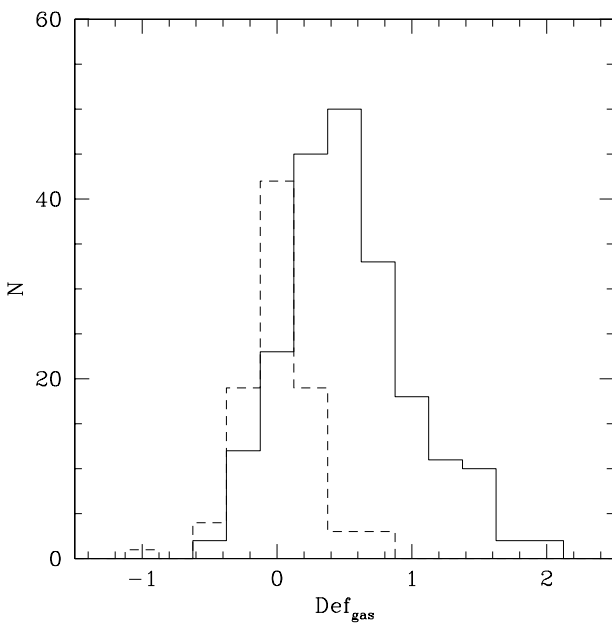


**Fig. 4.** Histograms of the  $Def_{gas}$  parameter for the isolated galaxies in the Coma supercluster (dashed line) and for Virgo galaxies (continuous line).

the  $Def_{gas}$  parameter are given in Fig. 4 for the Coma isolated objects and for the Virgo galaxies. Isolated objects have  $Def_{gas} = 0 \pm 0.18$ , while Virgo galaxies have significantly positive  $Def_{gas} = 0.53 \pm 0.35$ .

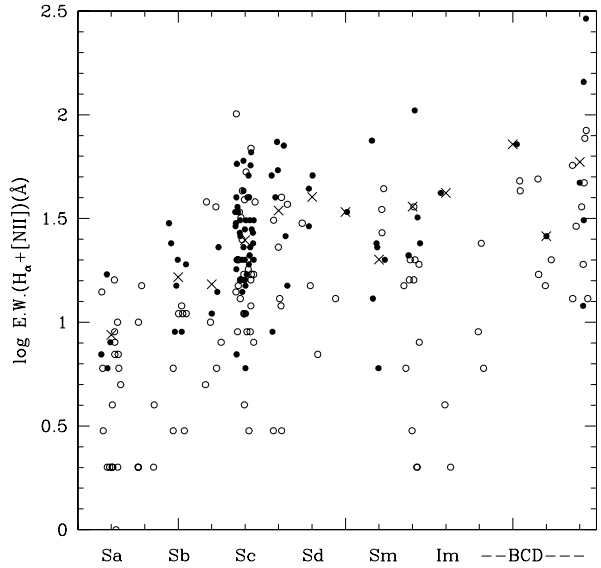


**Fig. 5.** The distribution of H $\alpha$  E.W. of spiral galaxies in the Virgo cluster as a function of Hubble type. Filled dots represent galaxies with normal gas content ( $Def_{gas} < 0.4$ ), open symbols are gas deficient objects. To avoid superposition of points, galaxies in each type bin are separated by a small random quantity. Crosses represent averages (including only the non gas-deficient galaxies) in each morphological type bin.

## 5. Results

The H $\alpha$  E.W. of galaxies is known to increase systematically along the Hubble sequence, from virtually zero for the early types (E-S0) to several hundred Å for the latest types (Kennicutt 1998). A weak trend is confirmed when data limited to the Virgo spiral galaxies included in this work are used, as shown in Fig. 5. However the scatter in each of the morphological type bins is as much as an order of magnitude, even though the scatter is somewhat reduced when gas deficient galaxies are excluded. The Hubble type alone does not account for the star formation properties of galaxies in this cluster. To shed light on other possible dependences we will analyze how the SFR varies as a function of the projected clustercentric distance (sect. 5.1), of the luminosity (sect. 5.2) and of the gaseous content of galaxies (sect. 5.3).

### 5.1. The clustercentric dependence of the SFR

Lewis et al. (2002) analyzed the dependence of the galaxy SFR on the projected distance from clusters in the 2dF survey. Their volume limited samples comprise galaxies of all morphological types with  $0.05 < z < 0.1$ , brighter than  $M_b < -19$ . They showed with high statistical significance that the median SFR of galaxies decreases with decreasing projected distance from clusters.

It would be interesting to compare these intermediate distance clusters with the 3 local clusters analyzed in this work, however a direct comparison cannot be carried out because data of early-type galaxies are not in our possession. The dependence of the  $H_\alpha$  E.W. on the clustercentric distance in units of virial radii can be analyzed only for the late-types galaxies, bearing in mind that our completeness is 60 %. We compute  $R_{virial} = 0.002\sigma_r h^{-1}$  (Girardi et al. 1998) for the 3 clusters assuming  $\sigma_r = 775, 840, 925$  km sec $^{-1}$  for Virgo, A1367 and Coma respectively. The combined Coma and A1367 clusters (with  $M_b < -19$ ) are shown in Fig. 6 embedded in the Coma supercluster that we trace out to large clustercentric radial distances. We find a significant inner decrease only of the 25<sup>th</sup> percentile of the  $H_\alpha$  E.W. distribution. Both the median and the 75<sup>th</sup> percentile instead increase inwards. We find it unlikely that the  $H_\alpha$  E.W. distribution is biased toward high values due to incompleteness, since for the Coma+A1367 clusters our survey covers 75 % of the sample. These clusters are inhabited by strong  $H_\alpha$  emitters to which the attention has been drawn by several authors. These include the "blue galaxies in the Coma cluster" of Bothun & Dressler (1986) and the blue galaxy sample observed with ISO by Contursi et al. (2001). Many (13) galaxies with  $H_\alpha$  E.W. in excess of 50 Å are found both in the inner regions ( $R/R_{virial} < 0.5$ ) and at intermediate distances ( $0.5 < R/R_{virial} < 1.5$ ) from the observed clusters. Noticeably these galaxies are near the faint limit of our survey ( $-19.5 < M_b < -19$  mag).

For the Virgo cluster we separate the bright sample ( $M_p < -19$ ), with a luminosity cutoff and  $H_\alpha$  completeness similar to the Coma supercluster (75 %), from the total sample ( $M_p < -15$ ) and we show the two radial dependences separately in Fig. 7. The bright sample shows an inner decrease of the SFR. For the total sample this pattern no longer holds true. The Virgo cluster contains 24 galaxies with  $H_\alpha$  E.W. in excess of 50 Å (11 are BCDs), the majority (14/24 objects) being fainter than -17.1 mag.

Because of their low optical luminosity the strong  $H_\alpha$  emitters belonging to Virgo would have all escaped detection in the 2dF survey. We conclude that, beside morphology segregation, the three local clusters analyzed in this work do not show a clear radial trend of the SFR distribution. The presence of the radial trend depends purely on a luminosity cutoff, which varies cluster to cluster between -17 and -19 mag. While spiral galaxies brighter than this cutoff luminosity have lower than average SFR at the cluster centers, galaxies fainter than this limit have SFR independent from the clustercentric projected distances. This is consistent with the idea that infall of small galaxies is occurring onto rich clusters at the present cosmological epoch.

## 5.2. The SFR in the Coma supercluster

Since, as concluded in the previous section, the present star formation rate of galaxies near the center of the stud-

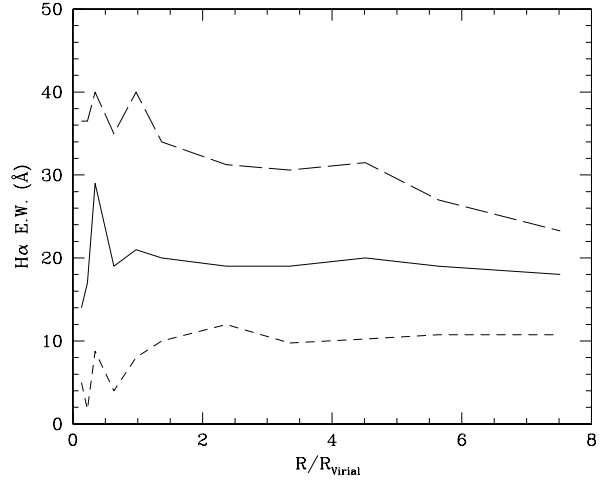


**Fig. 6.** The distribution of  $H_\alpha$  E.W. as a function of (projected) clustercentric radius from the Coma and A1367 clusters ( $M_b < -19$ ). The top and bottom lines represent the 75<sup>th</sup> and the 25<sup>th</sup> percentile of the EW distribution, while the central line is the median of the distribution.

ied clusters is a luminosity sensitive parameter, it is compelling to proceed to a systematic investigation of the luminosity dependence of the star formation properties. To this aim it is adequate to analyze the luminosity dependence of the birthrate parameter  $b$  (see section 4.1). The most appropriate luminosity indicator, which we will adopt hereafter, is the NIR (H band) luminosity. This parameter traces at best the dynamical mass (within the optical disk) of spiral galaxies, as concluded by Gavazzi et al. (1996c), who found  $\text{Log}M_{dyn} = \text{Log}L_H + 0.66$ . The dependence of the  $b$  parameter on  $L_H$ , given in Fig. 8, shows that the star formation history of spiral galaxies in the Coma supercluster region is in almost inverse proportionality with the system luminosity (mass). The most massive spirals ( $\text{Log}L_H \sim 11.5 L_H \odot \sim 12.3 M_\odot$ ) have their  $b$  parameter as much as 100 times lower than less luminous (giant) galaxies ( $\text{Log}L_H \sim 10 L_H \odot \sim 10.8 M_\odot$ ). This confirms previous claims that the current SFR, as derived from the  $H_\alpha$  E.W., anti-correlates with the system mass (Gavazzi et al. 1998). Furthermore Fig. 8 shows that there is not a significant difference between the SFH of galaxies in the rich Coma+A1367 clusters and of relatively isolated objects in the same supercluster, in agreement with Gavazzi et al. (1998).

Both results are however biased by selection effects. The Coma supercluster galaxies were selected optically in the blue (photographic) band ( $m_p \leq 15.7$ ). The selected targets were observed "a posteriori" in  $H_\alpha$  and in the NIR, therefore at any given  $L_H$  only galaxies bluer than a cer-

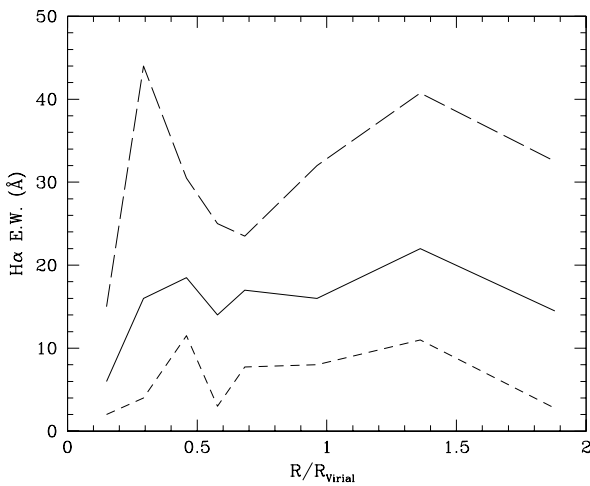
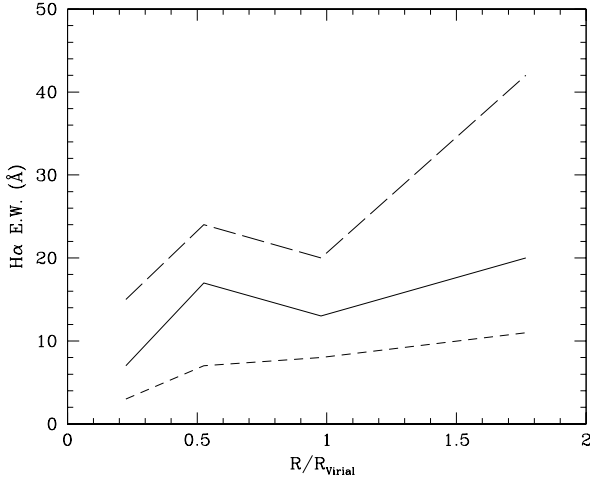


**Fig. 7.** The distribution of  $H_{\alpha}$  E.W. as a function of (projected) clustercentric radius from the Virgo cluster. The top and bottom lines represent the 75<sup>th</sup> and the 25<sup>th</sup> percentile of the EW distribution, while the central line is the median of the distribution. The top panel shows the Virgo galaxies brighter than  $M_p = -19$ , while the bottom panel includes all galaxies surveyed in  $H_{\alpha}$  ( $M_b < -15$ ).

tain threshold are sampled. In other words the B selection biases against faint-red galaxies, according to the relation between B-H and the infrared luminosity represented by equation 9 (see Scodéggi et al. 2002). This, combined with the fact that  $b$  correlates with the B-H color (see equation 10), introduces a selection effect in the  $b$  vs.  $L_H$

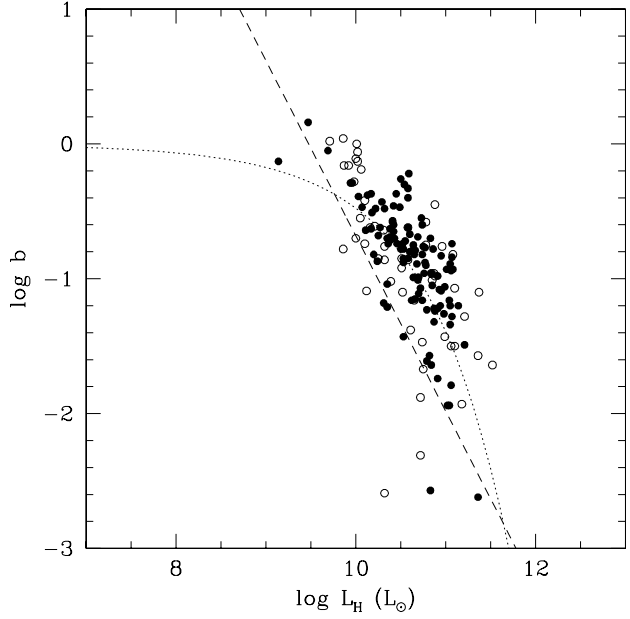


**Fig. 8.** The relation between the birthrate parameter and the NIR luminosity (mass) for the Coma supercluster galaxies. Galaxies in the Coma+A1367 clusters are represented with empty symbols, filled symbols are non-cluster galaxies. The dotted line represents the expected  $b$  as a function of  $L_H$  in the closed-box model of equation (5). The dashed line represents the observational bias affecting the Coma galaxies due to their selection in the B band.

plane (see equation 11). These empirically determined relations are:

$$B_{lim} - H = -12.7 - 5 \log(dist) + 2.5 \log L_H \quad (9)$$

where  $B_{lim} = -19.2$  corresponds to the limiting magnitude ( $m_p \leq 15.7$ ) at the Coma distance that we assume 96 Mpc.

$$\log b = 0.56 - 0.52(B - H) \quad (10)$$

$$\log b = 7.16 + 2.6 \log(dist) - 1.3 \log L_H \quad (11)$$

Equation 11 is represented in Fig. 8 with a dashed line. In conclusion, faint-low star forming galaxies at the distance of Coma below the diagonal line of Fig. 8 are severely undersampled.

### 5.3. The SFR in the Virgo cluster

The selection effect mentioned above affects the Virgo sample to a much lesser extent, because Virgo is 3.7 magnitudes closer than Coma. When we consider the Virgo galaxies alone in Fig. 9 we include dwarf systems with  $L_H$  fainter by almost 2 orders of magnitudes with respect to Coma. The scatter of the  $b$  vs.  $L_H$  relation increases considerably because the large majority of faint Virgo objects have  $b$  lower than Coma. This is in agreement with

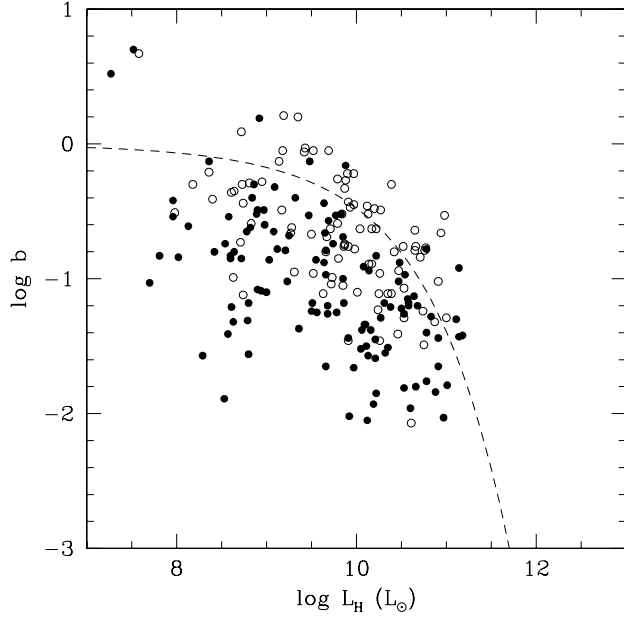


**Fig. 9.** The relation between the birthrate parameter and the NIR luminosity (mass) for the Virgo galaxies. Empty symbols represent galaxies with normal gas content ( $Def_{gas} < 0.4$ ) while deficient galaxies ( $Def_{gas} > 0.4$ ) are given with filled symbols.

Kennicutt (1983) who found evidence for significant  $H_\alpha$  deficiency in 12 Virgo galaxies with respect to isolated galaxies. Galaxies with  $b$  as low as the ones in Virgo might exist in the Coma+A1367 clusters as well, but are not observed because of the previously mentioned observational bias. Thus we conclude that, at any given mass, spirals belonging to the Virgo cluster have their present star formation activity significantly lower than isolated galaxies. It remains to be explained why. The first thing to explore is whether their gaseous content is sufficient for fueling the star formation. Cluster spirals are in fact known to suffer from HI deficiency (Giovanelli & Haynes 1985; Solanes et al. 2001), a pattern that is interpreted in the framework of the ram pressure mechanism (Gunn & Gott, 1972). When galaxies are separated according to their gas deficiency parameter (see Fig. 9), we recognize that, at any given  $L_H$ , galaxies with "normal" gas content ( $Def_{gas} < 0.4$ ) (open symbols) have their  $b$  parameter significantly

**Table 2.** The  $M_{gas}$  vs. diameter relation for isolated galaxies

Type	a	b	$R^2$
Sa – Sb	7.62	1.55	0.75
Sbc – Sc	7.48	1.68	0.75
Scd – Irr	7.74	1.49	0.77

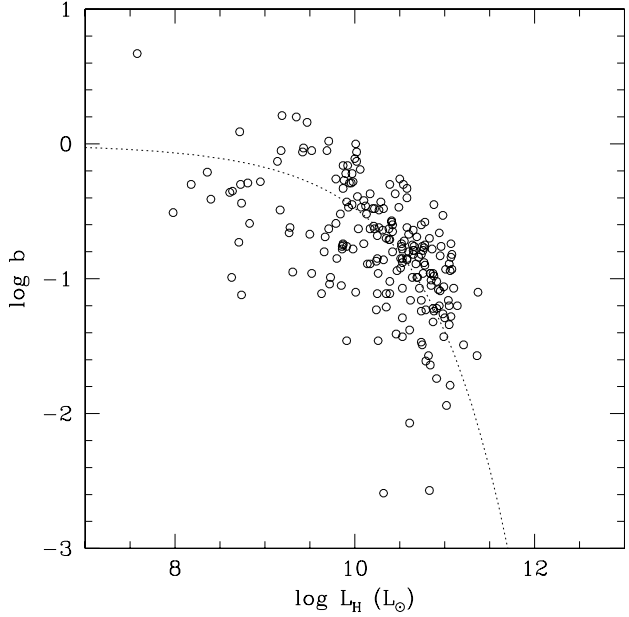


**Fig. 10.** The relation between the birthrate parameter and the NIR luminosity (mass) for Virgo+Coma galaxies with normal gas content ( $Def_{gas} < 0.4$ ).

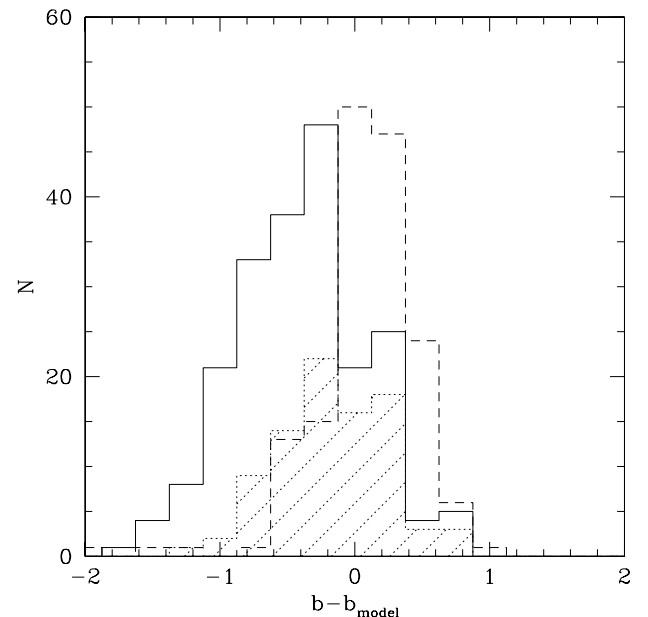


**Fig. 11.** Histograms of the residual  $b_{obs} - b_{mod}$  for the Coma galaxies (dashed line), for Virgo (continuous line) and for the Virgo galaxies with normal HI content ( $Def_{gas} < 0.4$ ) (dashed histogram).

higher than gas "deficient" objects.

Fig. 10 is restricted to the non deficient galaxies of both the Virgo and Coma regions. In this and in the previous figures the dotted curve represents  $b_{mod}$  i.e. the  $b$  vs.  $L_H$

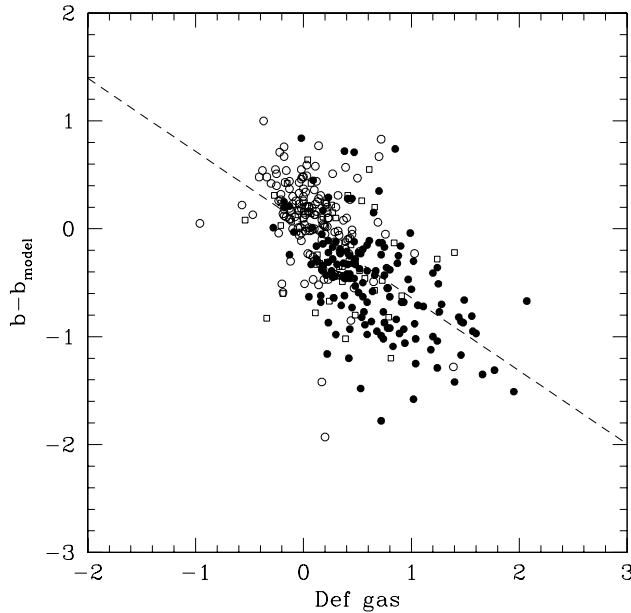


**Fig. 12.** The relation between  $b_{obs} - b_{mod}$  and the  $Def_{gas}$  parameter. Empty circles are Coma supercluster galaxies, empty squares are "normal" Virgo clouds (N, W, S), filled circles are "deficient" Virgo clouds (A, B, E).

relation expected from the closed-box scenario, in the assumption that  $\tau$  is inversely proportional to  $L_H$  according to equation (6). Galaxies in Fig. 10 are found in relatively good agreement with  $b_{mod}$ , in other words their residuals  $b_{resid} = b_{obs} - b_{mod}$  are small. This is evidenced in the histograms of Fig. 11 where the distribution of the residuals  $b_{resid} = b_{obs} - b_{mod}$  is given separately for the Coma galaxies, for the Virgo galaxies and for the subsample of the Virgo galaxies with normal gas content ( $Def_{gas} < 0.4$ ). Large negative residuals, implying a factor of 3 lower SFR, are associated with significantly gas deficient galaxies. It is concluded that, at any given luminosity, the principal parameter regulating the current star formation activity in cluster spirals is the availability of gas at their interior. This is further evidenced in Fig. 12, where  $b_{resid}$  is plotted against the gas deficiency parameter, showing a significant linear anti-correlation:  $b_{resid} = 0.04 - 0.68 \times Def_{gas}$ .

## 6. Discussion and conclusions

We have shown that a large fraction of late-type galaxies in the Virgo cluster have their current star formation rate significantly quenched with respect to isolated objects. These systems coincide with the Virgo gas deficient galaxies. Since the "gas" deficiency parameter is dominated by the HI phase (H<sub>2</sub> contributes only to 15 % of the HI), it is concluded that, to the first order, the star formation properties of galaxies in the Virgo cluster are determined by the pattern of HI deficiency. As earlier recognized by Kennicutt (1998), this is a somewhat surpris-

ing result, because the typical scales of HI and of star formation are very different in disk galaxies. HI reservoirs extend some 2 x the scale where the star formation takes place (Cayatte et al. 1994). We will re-examine this issue in more details in our forthcoming paper dedicated to the morphology of the star formation regions in galaxies, where a comparison between the scale-length of  $H_\alpha$ , HI and  $H_2$  will be carried on specifically. Limiting ourself to the global quantities, they indicate that infall of HI gas occurs in the disks on time scales similar to the star formation time. If the gas replenishment fails, because the HI reservoir is reduced by some ablation mechanism (e.g. ram pressure), the star formation adjusts itself to significantly lower rates.

Galaxies with  $b_{resid} < -0.7$  and  $Def_{gas} > 0.4$  ("quenched") are plotted in Fig. 13 with empty symbols, together with their "healthy" counterparts (filled symbols). Beside a marginal clustering of deficient objects around M87 (cluster A) and M49 (cluster B) the two populations appear mixed in position. There is for example a considerable fraction of "healthy" objects projected onto the center of cluster A. However Virgo is known to be a complex dynamical entity, composed by the main cluster (A) a secondary cluster (B), several Mpc behind A, and a number of clouds at approximately the distance of A, but with significantly discrepant velocities, suggesting infall (see Gavazzi et al. 1999a).

By considering galaxies with projected angular separation  $< 3.7$  deg from M87 we isolate 68 bona fide members of cluster A. We divide them into 48 "quenched" and 20 "healthy". For a considerable fraction (22/48 and 13/20 respectively) their distance is available from Gavazzi et al. (1999a) based on the H band Tully-Fisher relation (Tully & Fisher 1977) (distances of few galaxies whose H magnitudes were not yet available to Gavazzi et al. 1999a were recomputed by us). To our surprise we find that, while the average distance modulus of the deficient objects ( $\mu_o = 30.85$ ) is in perfect agreement with the distance modulus of cluster A as a whole ( $\mu_o = 30.82$ ) (Gavazzi et al. 1999a), the distance modulus of the non-deficient galaxies projected onto A is  $\mu_o = 31.77$  on average, thus almost one mag more distant. It is thus concluded that "healthy" spirals projected onto the Virgo center belong in fact to a background cloud with a distance comparable with that of cluster B. This cloud has not yet entered the dense environment of cluster A.

## 7. Summary

- We have covered with H $\alpha$ +[NII] and NIR imaging observations  $\sim 60\%$  of the late-type (spiral) galaxies brighter than  $m_p = 16.0$  in the Virgo cluster and in the Coma/A1367 supercluster.
- The H $\alpha$  E.W. of spiral galaxies shows the expected decrease toward the center of the three studied clusters only when galaxies brighter than -19.5 are considered. Weaker and dwarf systems show no or reverse trends,

Technology, under contract with the National Aeronautics and Space Administration.

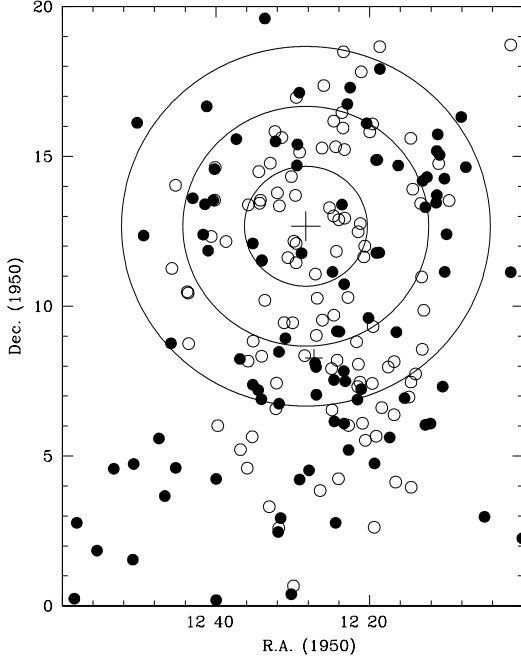


**Fig. 13.** The distribution of the "quenched" (empty symbols) and "healthy" (filled symbols) galaxies in the Virgo cluster. Positions of M87 and M49 are shown by crosses.

indicating that substantial infall of small spiral galaxies is currently taking place onto local clusters.

- From the combined H $\alpha$  and NIR data we derive the birthrate, i.e. the fraction of young to old stars, providing an estimate of the star formation history for these galaxies.
- The birthrate parameter shows a weak increasing trend with increasing lateness in the Hubble classification.
- The birthrate parameter of isolated galaxies in the Great Wall is in almost inverse proportionality with the NIR luminosity, i.e. with the systemic mass. Giant spiral galaxies have a ratio of young-to-old stars 100 times lower than their dwarf counterparts.
- A large fraction of spiral galaxies in the Virgo cluster have a birthrate parameter significantly lower (a factor 3) than isolated galaxies of similar luminosity.
- Galaxies with quenched current star formation coincide with galaxies with significant gas deficiency.
- A population of currently star forming galaxies with normal gas content is found projected near the center of the Virgo cluster. Their Tully-Fisher distance is approximately 1 mag larger than the one of the deficient objects, which corresponds with the distance of the M87 cluster. This points out the existence of a distinct cloud of galaxies falling onto the Virgo cluster.

**Acknowledgements.** This research has made use of the NASA/IPAC Extragalactic Database (NED) which is operated by the Jet Propulsion Laboratory, California Institute of

## References

- Almoznino E., & Brosch N., 1998, MNRAS, 298, 920A  
 Binggeli B., Sandage A., & Tammann G., 1985, AJ, 90, 1681 (VCC)  
 Binggeli B., Popescu C., & Tammann G., 1993, A&AS, 98, 275  
 Boselli A., Tuffs R. J., Gavazzi G., Hippelein H., & Pierini D., 1997, A&AS, 121, 507  
 Boselli A., Gavazzi G., Franzetti P., Pierini D., & Scoddeggio M., 2000, A&AS, 142, 73  
 Boselli A., Gavazzi G., Donas J., & Scoddeggio M., 2001, AJ, 121, 753  
 Boselli A., & Gavazzi G., 2002, A&A, 386, 124 (paper II)  
 Boselli A., Lequeux J., & Gavazzi G., 2002a, A&A, 384, 33  
 Boselli A., Iglesias J., Vilchez J., & Gavazzi G., 2002b, A&A, 386, 134 (paper III)  
 Bothun G. D., & Dressler A., 1986, ApJ, 301, 57  
 Cayatte V., Kotanyi C., Balkowski C., & van Gorkom J., 1994, AJ, 107, 1003  
 Contursi A., Boselli A., Gavazzi G., Bertagna E., Tuffs, R., & Lequeux J., 2001, A&A, 365, 11  
 Dressler A., 1980, ApJ, 236, 351  
 Gavazzi G., Boselli A., & Kennicutt R., 1991, AJ, 101, 1207  
 Gavazzi G., & Boselli A., 1996, Astro. Lett. & Comm., 35, 1  
 Gavazzi G., Pierini D., Boselli A., & Tuffs R., 1996a, A&AS, 120, 489  
 Gavazzi G., Pierini D., Baffa C., Lisi F., Hunt L. K., Randone L., & Boselli A., 1996b, A&AS, 120, 521  
 Gavazzi G., Pierini D., Boselli A., 1996c, A&A, 312, 397  
 Gavazzi G., Catinella B., Carrasco L., Boselli A., & Contursi A., 1998, AJ, 115, 1745  
 Gavazzi G., Boselli A., Scoddeggio M., Pierini D., & Belsole E., 1999a, MNRAS, 304, 595  
 Gavazzi G., Carrasco L., & Galli R., 1999b, A&AS, 136, 227  
 Gavazzi G., Franzetti P., Scoddeggio M., Boselli A., & Pierini D., 2000b, A&A, 361, 863  
 Gavazzi G., Franzetti P., Scoddeggio M., Boselli A., Pierini D., Baffa C., Lisi F., & Hunt L.K., 2000a, A&A, 342, 65  
 Gavazzi G., Zibetti S., Boselli A., Franzetti P., Scoddeggio M., & Martocchi S., 2001, A&A, 372, 29  
 Gavazzi G., Boselli A., Pedotti P., Gallazzi A., & Carrasco L., 2002a, A&A, 386, 114 (paper I)  
 Giovanelli R., & Haynes M., 1985, ApJ, 292, 404  
 Girardi M., Giuricin G., Mardirossian F., Mezzetti M., & Boschin W., 1998, ApJ, 505, 74  
 Gunn J.E., & Gott J.R.III, 1972, ApJ, 176, 1  
 Haynes M., & Giovanelli R., 1984, AJ, 89, 758  
 Heller A., Almoznino E., & Brosch N., 1999, MNRAS, 304, 8  
 Hoffman G. L., Salpeter E. E., Farhat B., Roos T., Williams H., & Helou G., 1996, ApJS, 105, 269  
 Iglesias J., Boselli A., Cortese L., Vilchez, J., & Gavazzi G., 2002, A&A, 384, 383  
 Kennicutt R., 1983, AJ, 88, 483  
 Kennicutt R., 1989, ApJ, 344, 685  
 Kennicutt R., Tamblyn P., & Congdon C., 1994, ApJ, 435, 22  
 Kennicutt R., 1998, ARA&A, 36, 189  
 Kennicutt R., Bothun G., & Schommer R., 1984, AJ, 89, 1279  
 Kennicutt R., & Kent S., 1983, AJ, 88, 1094  
 Koopmann R., Kenney J., & Joung J., 2001, ApJS, 135, 125  
 Lewis I. et al., 2002, MNRAS, 334, 673

- Mayer L., Governato F., Colpi M., Moore B., Quinn T., Wadsley J., Stadel J., & Lake G., 2001, ApJ, 559, 754
- Moore B., Katz N., Lake G., Dressler A., & Oemler A., 1996, Nature, 379, 613
- Moore B., Lake G., & Katz N., 1998, ApJ, 495, 139
- Moss C., Whittle M., & Pesce J., 1998, MNRAS, 300, 205
- Romanishin W., 1990, AJ, 100, 373
- Scodéggi M., & Gavazzi G., 1993, ApJ, 409, 110
- Scodéggi M., Gavazzi G., Franzetti P., Boselli A., Zibetti S., & Pierini D., 2002, A&A, 384, 812
- Solanes J. M., Manrique A., Garca-Gomez C., Gonzalez-Casado G., Giovanelli R., & Haynes M.P., 2001, ApJ, 548, 97
- Tully, B., & Fisher, J., 1977, A&A, 54, 661
- Usui T., Saito M., & Tomita A., 1998, AJ, 116, 2166
- Young J., Allen L., Kenney J., Lesser A., & Brooks R., 1996, AJ, 112, 1903
- Zwicky F., Herzog E., Karpowicz M., Kowal C., & Wild P., 1961-1968, "Catalogue of Galaxies and of Cluster of Galaxies" (Pasadena, California Institute of Technology; CGCG)

Table 3: The newly observed galaxies

VCC/CGCG (1)	NGC/IC (2)	UGC (3)	RA (J2000) (4)	Dec (5)	$m_{pg}$ (6)	Vel (7)	$T_{on}$ (8)	$R_{ON}$ (9)
343	3148	-	121921.68	075213.8	15.1	2479	20	0.79
841	-	-	122547.40	145711.4	15.6	501	20	0.66
15031	4771	8020	125321.85	011613.5	13.3	1119	15	0.85
15049	4845	8078	125801.33	013430.3	12.9	1097	15	0.85
15055	4904	8121	130058.89	-000142.4	13.2	1174	15	0.85
41041	4116	7111	120736.33	024133.1	13.0	1309	15	0.85
43028	4688	7961	124746.67	042005.3	14.5	984	15	0.84
43034	4701	7975	124911.87	032324.5	13.1	727	15	0.79
43054	4765	8018	125314.52	042749.4	13.0	725	15	0.79
69036	4067	7048	120411.46	105114.8	13.2	2424	15	0.8
100015	4758	8014	125244.16	155050.9	14.1	1240	15	0.85
157075	-	-	115940.06	263248.7	15.7	6694	15	0.77
160121	-	8161	130329.11	263300.8	15.5	6676	20	0.77

Table 4: Parameters of the analyzed galaxies

Gal (1)	Agg (2)	Type (3)	Virgo							ref (10)
			$\Theta$ Deg. (4)	H mag (5)	Dist. Mpc (6)	$Def_{gas}$ (7)	$H_{\alpha} + [NII]$ E.W. Å (8)	$LogF(H_{\alpha})$ erg cm $^{-2}$ s $^{-1}$ (9)		
VCC0001	$V_M$	BCD	5.63	12.75	32	-	12	-13.46	11	
VCC0010	$V_M$	BCD	5.35	12.76	32	0.34	31	-12.98	6	
VCC0017	$V_M$	Im	5.43	14.12	32	0.26	105	-12.78	9	
VCC0025	$V_M$	Sc	6.10	9.96	32	-0.15	58	-11.50	11	
VCC0047	$V_M$	Sa	4.62	10.70	32	0.79	16	-12.84	11	
VCC0058	$V_M$	Sb	4.48	10.51	32	0.15	15	-12.31	11	
VCC0066	$V_N$	Sc	4.68	9.01	17	-0.06	23	-11.45	1	
VCC0067	$V_M$	Sc	4.66	11.27	32	0.36	27	-12.49	7	
VCC0073	$V_W$	Sb	6.92	9.47	32	0.42	11	-12.19	11	
VCC0081	$V_N$	Sc	4.85	12.78	17	-0.19	21	-13.06	11	
VCC0083	$V_N$	Im	4.69	12.98	17	0.81	8	-13.73	6	
VCC0087	$V_N$	Sm	5.17	13.66	17	0.39	20	-12.89	7	
VCC0089	$V_M$	Sc	4.28	9.31	32	0.00	20	-11.73	1	
VCC0092	$V_N$	Sb	4.84	7.06	17	0.30	9	-11.33	7	
VCC0097	$V_M$	Sc	4.20	9.60	32	0.13	14	-12.13	11	
VCC0120	$V_W$	Scd	7.70	10.42	32	0.18	54	-11.87	11	
VCC0131	$V_N$	Sc	4.17	10.76	17	0.24	23	-12.48	11	
VCC0144	$V_W$	BCD	7.66	12.95	32	0.07	144	-12.19	12	
VCC0145	$V_N$	Sc	3.84	9.61	17	0.22	7	-11.84	7	
VCC0152	$V_N$	Scd	4.69	9.77	17	0.39	9	-12.59	7	
VCC0157	$V_N$	Sc	3.99	8.35	17	0.42	20	-11.43	1	
VCC0159	$V_W$	Im	5.54	13.23	32	0.57	19	-13.16	7	
VCC0162	$V_N$	Sd	4.06	11.48	17	0.48	30	-12.83	11	
VCC0167	$V_N$	Sb	3.72	6.69	17	0.66	3	-11.32	7	
VCC0199	$V_W$	Sa	6.05	8.86	32	0.84	10	-12.04	11	
VCC0213	$V_N$	BCD	3.60	11.52	17	0.66	24	-12.62	12	
VCC0221	$V_W$	Sc	9.35	11.23	32	0.54	53	-11.87	11	
VCC0222	$V_W$	Sa	6.19	8.73	32	0.91	2	-12.55	7	
VCC0226	$V_N$	Sc	4.42	8.89	17	-0.34	6	-12.23	1	
VCC0234	$V_W$	Sa	6.59	9.23	32	1.40	14	-12.11	7	
VCC0267	$V_B$	Sbc	6.55	10.92	23	0.16	11	-12.63	7	
VCC0307	$V_N$	Sc	3.55	7.20	17	0.04	29	-10.76	7	
VCC0318	$V_W$	Scd	4.57	12.97	32	0.04	51	-12.46	11	
VCC0324	$V_S$	BCD	9.01	11.83	17	0.70	57	-12.27	12	
VCC0328	$V_N$	Im	2.88	14.66	17	0.73	20	-13.62	9	
VCC0341	$V_B$	Sa	6.90	8.70	23	0.94	2	-12.66	7	
VCC0343	$V_A$	Sd	5.33	13.17	23	0.97	15	-13.37	T.W.	
VCC0382	$V_W$	Sc	7.55	9.31	32	-0.27	31	-11.58	7	
VCC0393	$V_B$	Sc	5.39	10.58	23	0.48	25	-12.14	11	
VCC0410	$V_N$	BCD	2.57	16.37	17	0.61	77	-13.25	6	
VCC0446	$V_B$	BCD	6.52	13.40	23	1.11	17	-13.43	7	
VCC0459	$V_A$	BCD	5.74	12.72	17	0.27	47	-12.61	12	
VCC0460	$V_A$	Sa	6.42	7.60	17	1.02	2	-11.65	1	
VCC0465	$V_N$	Sc	2.49	9.86	17	0.27	57	-11.43	11	
VCC0483	$V_A$	Sc	3.16	8.49	17	0.17	31	-11.41	7	
VCC0491	$V_N$	Scd	2.41	10.99	17	0.02	74	-11.67	4	
VCC0492	$V_B$	Sa	7.36	9.68	23	1.46	6	-12.54	11	
VCC0497	$V_A$	Sc	3.13	8.11	17	0.46	15	-11.66	7	
VCC0508	$V_S$	Sc	8.22	7.09	17	-0.02	34	-10.58	1	
VCC0513	$V_S$	BCD	10.28	12.33	17	1.24	47	-12.67	12	
VCC0524	$V_B$	Sbc	3.98	9.54	23	1.49	5	-12.32	7	

## Virgo cont.

Gal	Agg	Type	$\Theta$	H	Dist.	$Def_{gas}$	$H_{\alpha} + [NII]E.W.$	$LogF(H_{\alpha})$	ref
(1)	(2)	(3)	Deg.	mag	Mpc	(7)	$\text{\AA}$	$\text{erg cm}^{-2} \text{ s}^{-1}$	(10)
VCC0530	$V_A$	Im	4.01	15.02	17	1.26	3	-14.06	9
VCC0534	$V_B$	Sa	5.66	9.95	23	1.56	8	-12.54	11
VCC0559	$V_A$	Sab	3.74	8.99	17	1.04	2	-12.66	7
VCC0562	$V_A$	BCD	2.02	15.75	17	0.85	84	-12.82	6
VCC0576	$V_B$	Sbc	3.65	9.61	23	0.16	14	-12.29	11
VCC0596	$V_A$	Sc	3.93	6.69	17	0.47	18	-10.81	7
VCC0613	$V_S$	Sa	7.39	8.67	17	0.54	6	-12.20	11
VCC0620	$V_A$	Sm	1.99	13.02	17	0.83	27	-13.64	7
VCC0630	$V_A$	Sd	2.11	9.77	17	1.20	7	-12.57	7
VCC0641	$V_B$	BCD	6.82	13.87	23	0.55	19	-13.51	7
VCC0655	$V_A$	BCD	5.44	10.66	17	0.68	6	-12.73	12
VCC0656	$V_B$	Sb	5.72	9.34	23	0.40	9	-12.06	7
VCC0664	$V_A$	Sc	1.73	12.24	17	0.70	101	-11.92	7
VCC0667	$V_B$	Sc	5.49	10.76	23	0.75	9	-12.77	11
VCC0688	$V_B$	Sc	4.90	11.00	23	0.63	9	-12.82	11
VCC0692	$V_A$	Sc	1.67	10.44	17	0.78	16	-12.27	13
VCC0697	$V_B$	Sc	5.60	11.05	23	0.80	14	-12.61	7
VCC0699	$V_B$	Pec	6.02	10.93	23	0.27	42	-12.22	11
VCC0713	$V_B$	Sc	4.18	9.81	23	1.44	8	-12.52	11
VCC0768	$V_A$	Sc	4.83	12.30	17	0.41	43	-12.63	11
VCC0785	$V_S$	Sa	7.59	8.41	17	0.28	8	-11.99	11
VCC0787	$V_B$	Scd	6.79	11.08	23	0.48	31	-12.31	12
VCC0792	$V_B$	Sab	2.73	8.55	23	0.86	10	-12.44	7
VCC0793	$V_A$	Im	1.50	15.29	17	0.59	2	-14.36	12
VCC0801	$V_A$	?	4.28	9.63	17	-0.28	69	-11.52	7
VCC0802	$V_A$	BCD	1.71	14.64	17	0.77	36	-13.49	12
VCC0827	$V_B$	Sc	5.33	9.85	23	0.18	26	-12.05	11
VCC0836	$V_A$	Sab	1.26	8.21	17	0.73	15	-11.47	7
VCC0841	$V_A$	BCD	2.84	13.65	17	0.99	29	-13.08	T.W.
VCC0848	$V_B$	BCD	6.70	13.35	23	0.13	26	-13.00	12
VCC0849	$V_B$	Sbc	2.29	10.74	23	0.40	23	-12.10	4
VCC0851	$V_B$	Sc	4.99	10.71	23	0.38	20	-12.35	11
VCC0857	$V_A$	Sb	5.94	8.23	17	0.66	12	-11.77	7
VCC0865	$V_A$	Sc	3.48	10.33	17	0.51	34	-11.92	7
VCC0873	$V_A$	Sc	1.36	8.58	17	0.26	16	-11.76	12
VCC0874	$V_A$	Sc	3.96	9.63	17	0.42	3	-12.73	7
VCC0905	$V_B$	Sc	3.68	11.07	23	0.47	39	-12.44	7
VCC0912	$V_A$	Sbc	1.07	9.91	17	0.74	8	-12.36	7
VCC0921	$V_S$	Sbc	8.49	10.44	17	0.61	38	-11.83	11
VCC0938	$V_S$	Sc	4.58	10.20	17	0.52	20	-12.04	4
VCC0939	$V_B$	Sc	3.65	10.53	23	0.37	24	-12.17	4
VCC0950	$V_A$	Sm	1.28	12.98	17	0.23	23	-13.40	11
VCC0957	$V_S$	Sc	9.94	9.77	17	0.08	40	-11.55	1
VCC0958	$V_A$	Sa	2.82	8.03	17	0.22	7	-12.50	7
VCC0971	$V_B$	Sd	6.57	11.46	23	0.17	29	-12.47	11
VCC0975	$V_B$	Scd	5.21	11.06	23	0.39	26	-12.44	4
VCC0979	$V_B$	Sa	3.10	8.95	23	1.20	9	-12.02	7
VCC0980	$V_A$	Scd	3.61	12.45	17	0.88	40	-12.60	11
VCC0984	$V_A$	Sa	0.94	9.26	17	1.95	1	-12.97	7
VCC0995	$V_A$	Sc	1.75	13.03	17	-0.13	31	-12.79	7
VCC1002	$V_B$	Sc	6.19	9.65	23	0.53	9	-11.91	7
VCC1011	$V_S$	Sdm	4.82	12.30	17	0.78	13	-13.22	11
VCC1043	$V_A$	Sb	0.97	7.27	17	0.75	6	-11.57	13

## Virgo cont.

Gal	Agg	Type	$\Theta$ Deg.	H mag	Dist. Mpc	$Def_{gas}$	$H_\alpha + [NII]E.W.$ Å	$LogF(H_\alpha)$ erg cm $^{-2}$ s $^{-1}$	ref
(1)	(2)	(3)	(4)	(5)	(6)	(7)	(8)	(9)	(10)
VCC1110	$V_A$	Sab	4.73	7.13	17	0.93	2	-12.10	13
VCC1118	$V_B$	Sc	3.18	10.02	23	0.67	17	-12.14	11
VCC1126	$V_A$	Sc	2.66	9.39	17	1.48	11	-12.35	11
VCC1145	$V_S$	Sb	8.83	7.96	17	0.55	11	-11.53	7
VCC1179	$V_B$	BCD	2.43	13.25	23	1.25	20	-13.17	6
VCC1189	$V_S$	Sc	5.63	11.42	17	0.43	20	-12.47	7
VCC1190	$V_B$	Sa	3.66	8.27	23	2.07	3	-12.29	7
VCC1193	$V_S$	Sc	4.71	11.35	17	0.18	31	-12.38	11
VCC1200	$V_A$	Im	1.63	12.58	17	1.46	16	-13.56	7
VCC1205	$V_S$	Sc	4.58	10.23	17	0.05	11	-12.30	7
VCC1290	$V_S$	Sb	8.14	9.78	17	0.07	30	-11.89	11
VCC1313	$V_A$	BCD	0.35	15.60	17	0.38	291	-12.79	12
VCC1330	$V_S$	Sa	4.31	9.22	17	1.04	4	-12.48	11
VCC1356	$V_A$	BCD	0.91	13.10	17	0.43	43	-13.00	11
VCC1374	$V_A$	BCD	2.48	12.41	17	0.59	49	-12.48	6
VCC1375	$V_S$	Sc	8.45	11.17	17	0.09	28	-11.49	7
VCC1379	$V_A$	Sc	4.46	9.95	17	0.30	36	-11.72	11
VCC1393	$V_A$	Sc	2.74	10.87	17	0.43	38	-12.10	11
VCC1401	$V_A$	Sbc	2.05	6.60	17	0.41	6	-11.28	7
VCC1410	$V_A$	Sm	4.31	12.11	17	0.75	35	-12.66	11
VCC1411	$V_A$	Pec	0.65	13.83	17	0.53	2	-14.32	11
VCC1412	$V_A$	Sa	1.25	8.22	17	1.60	2	-12.32	7
VCC1419	$V_A$	S..	1.08	10.39	17	1.77	5	-13.02	7
VCC1426	$V_A$	Im	0.63	13.13	17	1.24	6	-13.88	11
VCC1437	$V_S$	BCD	3.25	12.21	17	0.43	13	-13.19	12
VCC1450	$V_A$	Sc	1.72	10.85	17	0.65	69	-11.69	7
VCC1486	$V_A$	S..	1.19	12.05	17	0.93	11	-13.14	7
VCC1508	$V_S$	Sc	3.79	9.73	17	-0.09	40	-11.58	11
VCC1516	$V_S$	Sbc	3.29	9.93	17	0.51	10	-12.19	13
VCC1532	$V_A$	Sc	3.06	10.68	17	1.00	17	-12.35	11
VCC1540	$V_S$	Sb	9.77	7.27	17	-0.18	20	-11.15	7
VCC1552	$V_A$	Sa	1.08	9.07	17	1.66	2	-12.78	7
VCC1554	$V_S$	Sm	5.99	9.79	17	-0.13	75	-11.35	13
VCC1555	$V_S$	Sc	4.28	7.64	17	0.23	17	-11.06	7
VCC1557	$V_S$	Scd	10.10	11.74	17	0.64	23	-12.69	11
VCC1562	$V_S$	Sc	10.24	7.78	17	0.18	20	-11.17	7
VCC1569	$V_A$	Scd	1.43	13.51	17	1.28	13	-13.42	7
VCC1575	$V_S$	Sm	5.32	11.27	17	0.35	13	-12.68	7
VCC1581	$V_S$	Sm	6.17	12.69	17	0.30	6	-13.41	11
VCC1585	$V_A$	Im	2.99	13.54	17	0.23	21	-13.04	9
VCC1588	$V_A$	Scd	3.31	9.43	17	0.74	3	-12.51	7
VCC1615	$V_A$	Sb	2.38	7.28	17	0.59	3	-11.78	1
VCC1624	$V_S$	Sc	9.43	10.35	17	0.80	11	-12.62	11
VCC1654	$V_A$	Im	2.79	14.22	17	0.48	20	-13.52	11
VCC1673	$V_A$	Sc	1.80	8.22	17	0.27	15	-11.80	7
VCC1675	$V_S$	Pec	4.56	12.56	17	1.40	4	-13.80	11
VCC1676	$V_A$	Sc	1.82	7.70	17	0.34	19	-11.54	7
VCC1678	$V_S$	Sd	5.94	12.52	17	0.18	51	-12.52	7
VCC1686	$V_A$	Sm	1.68	11.25	17	0.90	44	-12.12	11
VCC1690	$V_A$	Sab	1.65	7.02	17	0.80	2	-11.82	7
VCC1696	$V_A$	Sc	2.35	8.59	17	0.55	12	-11.86	4
VCC1699	$V_S$	Sm	5.68	12.47	17	0.36	24	-12.80	11
VCC1725	$V_S$	BCD	4.19	12.13	17	0.87	48	-12.56	12

Virgo cont.									
Gal	Agg	Type	$\Theta$	H	Dist.	$Def_{gas}$	$H_{\alpha} + [NII]E.W.$	$LogF(H_{\alpha})$	ref
(1)	(2)	(3)	Deg.	mag	Mpc	(7)	$\text{\AA}$	erg cm $^{-2}$ s $^{-1}$	(10)
VCC1726	$V_S$	Sdm	5.55	12.96	17	0.34	34	-12.75	7
VCC1727	$V_A$	Sab	1.78	6.77	17	0.45	4	-11.22	1
VCC1730	$V_S$	Sc	7.23	9.02	17	0.72	4	-12.42	7
VCC1757	$V_A$	Sa	1.96	10.81	17	1.57	7	-12.78	11
VCC1758	$V_S$	Sc	4.87	11.97	17	0.59	17	-12.87	11
VCC1760	$V_S$	Sa	8.29	8.74	17	1.03	5	-12.26	7
VCC1789	$V_S$	Im	7.74	12.95	17	0.91	16	-13.20	11
VCC1791	$V_S$	BCD	4.90	12.17	17	0.23	72	-12.37	11
VCC1811	$V_E$	Sc	3.64	9.92	17	0.28	11	-12.23	1
VCC1868	$V_E$	Scd	2.59	9.74	17	1.02	3	-13.13	7
VCC1918	$V_S$	Im	7.23	14.49	17	0.56	15	-13.85	11
VCC1923	$V_S$	Sbc	8.91	9.98	17	0.47	36	-11.73	11
VCC1929	$V_E$	Scd	3.48	10.78	17	0.57	12	-12.71	7
VCC1931	$V_E$	Im	3.02	13.04	17	0.45	36	-13.28	7
VCC1932	$V_E$	Sc	3.45	9.52	17	0.38	16	-12.13	7
VCC1943	$V_E$	Sb	3.06	8.90	17	0.31	24	-11.74	7
VCC1952	$V_E$	Im	5.62	14.60	17	0.29	32	-13.57	9
VCC1955	$V_E$	BCD	3.02	11.16	17	1.18	9	-13.05	12
VCC1972	$V_E$	Sc	3.21	8.38	17	0.12	16	-11.51	4
VCC1987	$V_E$	Sc	3.28	7.90	17	-0.18	30	-11.14	4
VCC1992	$V_E$	Im	3.27	14.10	17	0.23	24	-13.16	9
VCC2023	$V_E$	Sc	3.70	11.62	17	0.12	27	-12.36	11
VCC2033	$V_E$	BCD	5.42	13.06	17	1.06	13	-13.27	12
VCC2034	$V_E$	Im	4.36	13.23	17	0.72	2	-14.40	12
VCC2037	$V_E$	BCD	4.37	12.55	17	1.24	15	-13.42	7
VCC2058	$V_E$	Sc	4.34	8.37	17	0.72	13	-11.58	1
VCC2066	$V_E$	?	4.49	9.28	17	0.89	6	-12.43	7
VCC2070	$V_E$	Sa	5.82	7.68	17	0.21	6	-11.78	4
Z013046	$V_Z$	Sa	12.53	8.93	17	0.36	17	-11.90	10
Z014062	$V_Z$	Scd	12.01	10.47	17	0.11	15	-12.52	4
Z014063	$V_Z$	Sc	12.29	7.61	17	0.41	32	-11.04	7
Z014110	$V_Z$	Sc	12.81	9.23	17	-0.21	34	-11.43	1
Z015031	$V_Z$	Sc	12.44	9.2	17	0.52	16	-12.11	T.W.
Z015049	$V_Z$	Sb	12.74	8.13	17	1.24	11	-11.89	T.W.
Z015055	$V_Z$	Sc	14.5	9.46	17	0.33	28	-11.89	T.W.
Z041041	$V_Z$	Scd	11.28	9.88	17	0.00	40	-11.77	T.W.
Z043028	$V_Z$	Sc	9.08	10.74	17	0.21	60	-11.82	T.W.
Z043034	$V_Z$	Sc	10.08	10.07	17	-0.05	51	-11.77	T.W.
Z043041	$V_Z$	Sc	8.51	9.62	17	-0.21	66	-11.29	4
Z043054	$V_Z$	Scd	9.67	10.97	17	0.00	71	-11.90	T.W.
Z043071	$V_Z$	Sc	10.18	9.25	17	-0.54	43	-11.37	1
Z043093	$V_Z$	Sc	12.34	8.87	17	0.07	40	-11.25	1
Z069036	$V_Z$	Sb	6.7	10.38	17	0.33	19	-12.32	T.W.
Z071060	$V_Z$	Sd	5.16	9.87	17	0.12	44	-11.92	7
Z098044	$V_Z$	Sa	4.87	8.78	17	1.20	7	-11.91	13
Z099098	$V_Z$	Sc	10.22	11.69	17	-0.43	18	-12.02	1
Z100004	$V_Z$	Sc	5.07	8.25	17	-0.11	20	-11.27	1
Z100015	$V_Z$	Scd	6.34	10.13	17	0.44	37	-12.06	T.W.
Coma/A1367 supercluster									
Z097005	Iso	Sc	2.74	12.41	81	-0.18	39	-12.66	11
Z097026	Prs	Pec	1.77	11.65	83	-0.38	83	-12.18	11
Z097027	Prs	Sc	1.77	11.84	88	0.37	22	-12.69	11

## Coma/A1367 supercluster. Cont.

Gal	Agg	Type	$\Theta$	H	Dist.	$Def_{gas}$	$H_\alpha + [NII]E.W.$	$LogF(H_\alpha)$	ref
(1)	(2)	(3)	Deg.	mag	Mpc	(7)	$\text{\AA}$	$\text{erg cm}^{-2} \text{s}^{-1}$	(10)
(5)	(6)	(8)	(9)	(10)					
Z097062	A1367	Pec	0.53	12.94	91	0.34	37	-13.13	11
Z097063	A1367	Pec	0.55	13.56	91	0.18	22	-13.42	11
Z097064	A1367	S..	0.58	12.41	91	0.20	1	-14.77	11
Z097068	A1367	Sbc	0.55	11.26	91	-0.25	41	-12.30	1
Z097072	A1367	Sa	0.44	11.36	91	0.32	5	-13.23	2
Z097073	A1367	Pec	0.37	13.19	91	0.00	111	-12.60	11
Z097076	A1367	Sb	0.36	11.39	91	1.39	1	-14.08	11
Z097079	A1367	Pec	0.33	13.15	91	0.10	129	-12.61	11
Z097087	A1367	Pec	0.20	11.01	91	0.14	77	-12.07	5
Z097091	A1367	Sa	0.27	11.07	91	-0.05	23	-12.66	14
Z097092	A1367	Sbc	0.38	12.57	91	0.04	28	-13.10	1
Z097093	A1367	Pec	0.09	12.90	91	0.47	9	-13.47	5
Z097102	A1367	Sa	0.40	11.40	91	0.44	2	-13.66	5
Z097114	A1367	Pec	0.11	13.19	91	-	36	-13.19	14
Z097120	A1367	Sa	0.10	10.55	91	0.45	4	-12.93	2
Z097122	A1367	Pec	0.38	11.74	91	0.43	46	-12.53	2
Z097129N	A1367	Sb	0.22	9.77	91	-0.37	14	-12.23	5
Z097129S	A1367	Sbc	0.22	11.91	91	-	17	-13.08	5
Z097138	A1367	Pec	0.38	13.92	91	-0.13	64	-12.77	5
Z097149	A1367	S..	0.93	11.68	91	0.23	13	-13.26	3
Z097168	Iso	S..	1.81	12.41	80	0.42	78	-13.00	8
Z098002	Iso	Sb	2.32	13.13	82	0.12	34	-12.76	8
Z098013	Iso	Sc	3.49	11.73	92	-0.10	35	-12.58	5
Z098016	Iso	Sc	4.12	12.12	86	0.17	31	-12.70	5
Z098023	Prs	Sb	4.53	11.58	92	-	11	-13.00	5
Z098041	Grp	Sc	4.66	11.86	97	0.70	66	-12.18	3
Z098046	Grp	Sa	4.75	10.66	97	0.21	8	-12.76	3
Z098058	Iso	Sbc	5.50	10.70	96	0.00	11	-12.70	5
Z098081	Prs	Sa	6.52	11.57	96	-	14	-12.86	5
Z098085	Prs	Sc	6.64	12.05	94	-0.04	29	-12.50	3
Z098116	Iso	Sc	7.33	11.87	83	-0.25	39	-12.34	5
Z100005	Iso	Pec	9.85	10.66	88	0.32	19	-12.54	3
Z100012	Iso	Pec	10.10	12.47	86	-0.04	39	-12.89	5
Z101033	Iso	Sc	9.80	12.29	89	0.14	16	-13.34	11
Z101049	Iso	Sbc	10.09	11.49	95	-0.23	10	-12.88	11
Z101054	Iso	Sab	12.05	10.75	88	-0.04	11	-12.61	5
Z127005	Iso	Sbc	3.04	12.22	91	0.05	26	-12.82	5
Z127018	Iso	Sb	3.06	12.33	92	-	16	-12.89	3
Z127025S	Prs	Sbc	2.74	11.20	94	-0.02	22	-12.39	2
Z127025N	Prs	Sc	2.76	11.73	95	-	21	-12.70	3
Z127026	Iso	Sbc	6.01	11.30	91	-0.16	15	-12.70	11
Z127033	Iso	Sc	5.02	11.46	84	0.06	10	-12.96	5
Z127035	Iso	Sa	4.13	11.21	91	0.29	10	-12.93	5
Z127037	Iso	Pec	5.19	12.90	82	-0.00	47	-12.77	5
Z127038	Iso	Sc	2.91	10.54	92	-0.18	16	-12.27	2
Z127039	Iso	Sbc	3.20	12.16	92	-	48	-12.54	3
Z127049	A1367	Pec	0.87	11.93	91	0.29	57	-12.84	8
Z127050	Grp	Sbc	1.26	11.38	93	0.00	16	-12.53	2
Z127052	A1367	Sa	0.71	9.79	91	0.27	4	-12.70	5
Z127053	Iso	Sbc	4.18	11.33	85	-0.10	17	-12.74	5
Z127054	Grp	Sb	1.02	10.62	93	0.10	4	-12.81	5
Z127055	Iso	Pec	1.55	12.06	89	-	41	-12.74	8
Z127061	Iso	Sc	5.24	12.99	79	-0.12	29	-12.70	11

## Coma/A1367 supercluster. Cont.

Gal	Agg	Type	$\Theta$	H	Dist.	$Def_{gas}$	$H_\alpha + [NII]E.W.$	$LogF(H_\alpha)$	ref
(1)	(2)	(3)	Deg.	mag	Mpc	(7)	$\text{\AA}$	$\text{erg cm}^{-2} \text{ s}^{-1}$	(10)
			(4)	(5)	(6)		(8)		
Z127071	Grp	Pec	2.02	12.83	93	0.22	52	-12.71	3
Z127082	Grp	Sc	2.20	11.39	93	0.11	22	-12.59	2
Z127095	Grp	Sc	2.29	10.55	93	0.03	15	-12.36	2
Z127100	Grp	Sb	2.37	11.05	93	0.06	10	-12.87	2
Z128003	Iso	Pec	5.05	11.61	86	-0.07	41	-12.48	3
Z128015	Prs	Sb	5.01	11.96	91	-	21	-12.78	5
Z128016	Iso	S..	5.32	12.07	88	-0.13	35	-12.69	3
Z128021	Iso	Sbc	7.19	10.95	94	0.03	16	-12.68	5
Z128023	Grp	Sa	5.08	10.70	97	-0.16	17	-12.43	3
Z128049	Iso	Sc	8.58	11.31	86	0.41	20	-12.85	3
Z128063	Prs	Sa	7.56	11.07	90	0.19	4	-13.28	3
Z128072	Iso	Pec	9.20	12.26	91	-	37	-12.81	5
Z128073	Iso	Sb	9.52	11.29	92	-0.02	16	-12.63	5
Z128080	Iso	Sb	9.34	11.76	98	-0.13	24	-12.67	3
Z128087	Iso	Sc	8.02	11.55	89	0.20	14	-12.83	5
Z128089	Iso	Sa	9.15	10.76	91	0.40	9	-12.78	5
Z129004	Iso	S..	8.82	12.04	91	-	34	-12.77	5
Z129020	Iso	Sb	7.99	10.94	87	0.15	10	-12.81	5
Z129021	Iso	S..	7.60	11.83	89	-0.96	24	-12.72	3
Z129022	Iso	Sab	5.96	10.63	93	-0.10	8	-12.63	3
Z130003	Iso	Sb	6.17	11.01	95	-	19	-12.60	5
Z130005	Iso	Sbc	5.77	12.24	94	0.22	40	-12.69	11
Z130006	Iso	Sbc	2.35	11.45	87	-0.04	32	-12.59	5
Z130008	Iso	Sc	2.89	11.89	97	-0.41	49	-12.37	2
Z130014	Iso	Sbc	4.07	11.36	94	0.05	20	-12.64	3
Z130021	Iso	Sa	4.31	11.57	95	0.16	28	-12.54	5
Z130025	Iso	Sa	7.10	11.18	93	0.17	1	-14.26	11
Z130026	Prs	Sc	8.34	11.59	91	0.02	18	-12.67	11
Z130029	Prs	Sc	8.40	11.35	90	-	54	-12.31	11
Z131008	Iso	Sbc	9.48	11.16	79	-0.03	27	-12.67	11
Z131009	Iso	Sc	7.40	12.39	100	0.05	27	-12.74	5
Z157012	Iso	Sbc	9.08	12.40	91	-0.18	30	-12.65	3
Z157032	Iso	Sa	9.78	9.79	91	0.78	1	-13.75	5
Z157035	Iso	Sb	10.57	10.34	83	-0.18	19	-12.09	3
Z157044	Iso	Pec	7.14	12.86	88	-	40	-13.00	5
Z157062	Iso	Pec	11.64	14.53	92	0.12	77	-12.87	11
Z157064	Iso	Sb	9.71	11.72	85	-0.02	11	-12.79	5
Z157075	Iso	Sc	7.58	12.97	89	0.18	29	-13.14	T.W.
Z158009	Prs	Sb	12.24	10.77	100	0.11	17	-12.41	3
Z158010	Prs	Sbc	12.23	12.07	105	0.19	22	-12.89	3
Z158036	Iso	Sb	8.89	10.24	87	-0.17	11	-12.51	5
Z158038	Iso	Sab	11.23	11.66	90	0.23	23	-12.68	3
Z158054	Iso	Pec	9.86	12.01	102	-0.02	72	-12.35	3
Z158081	Iso	Pec	9.15	11.85	90	0.02	24	-12.80	3
Z158105	Iso	Sbc	7.93	11.50	91	-0.12	17	-12.71	5
Z159008	Iso	Sb	6.71	10.98	98	0.03	24	-12.44	5
Z159031	Prs	Sa	5.09	11.55	100	-0.02	9	-12.99	3
Z159033	Iso	Sa	4.98	10.85	102	0.65	2	-13.50	5
Z159037	Iso	Sab	4.86	11.50	97	-0.13	44	-12.42	11
Z159040	Iso	Sa	5.14	12.20	93	-0.19	26	-12.69	3
Z159059	Iso	Sab	3.73	12.15	100	-0.26	61	-12.34	5
Z159061	Iso	Sbc	4.77	11.18	93	0.29	4	-13.26	5
Z159071	Iso	Sc	3.43	12.78	92	-	32	-12.84	11

## Coma/A1367 supercluster. Cont.

Gal	Agg	Type	$\Theta$	H	Dist.	$Def_{gas}$	$H_\alpha + [NII]E.W.$	$LogF(H_\alpha)$	ref
(1)	(2)	(3)	Deg.	mag	Mpc	(7)	$\text{\AA}$	$\text{erg cm}^{-2} \text{ s}^{-1}$	(10)
			(4)	(5)	(6)	(7)	(8)	(9)	
Z159072S	Prs	Pec	4.06	10.84	88	0.01	12	-12.77	11
Z159072N	Prs	Pec	4.07	10.85	88	0.09	4	-13.30	11
Z159076	Iso	Sbc	3.27	11.08	90	0.30	15	-12.61	2
Z159090	Prs	Sc	2.05	12.25	111	-0.47	22	-12.83	2
Z159091	Iso	S..	2.17	11.74	86	-0.19	6	-13.34	3
Z159095	Iso	Sbc	3.60	11.23	91	-0.20	4	-13.32	5
Z159096	Iso	Sc	3.82	12.10	82	0.08	22	-12.76	5
Z159097	Iso	Pec	1.98	12.22	86	-	18	-13.15	5
Z159101	Coma	Pec	1.67	13.50	96	0.14	64	-12.78	5
Z159102	Coma	Sab	1.60	10.60	96	-0.22	31	-12.28	5
Z160001	Coma	Sb	1.66	12.34	96	0.10	15	-13.17	11
Z160005	Iso	Sb	2.07	10.47	84	0.01	3	-13.35	5
Z160009	Coma	S..	1.25	11.44	96	-	6	-13.46	11
Z160020	Coma	Pec	0.90	13.36	96	0.08	33	-12.84	5
Z160025	Coma	Sa	1.25	10.35	96	1.03	2	-13.29	5
Z160026	Coma	Sc	1.03	12.53	96	0.20	35	-12.87	5
Z160032	Coma	Sb	1.64	11.69	96	0.52	10	-13.05	5
Z160055	Coma	Sab	0.48	10.91	96	0.39	31	-12.34	14
Z160058	Coma	Sbc	0.82	11.87	96	0.22	22	-12.82	2
Z160064	Coma	Pec	0.77	12.79	96	0.32	67	-12.94	5
Z160067	Coma	Pec	0.85	13.16	96	-0.21	78	-12.67	5
Z160073	Coma	Pec	0.38	12.50	96	0.43	23	-12.98	5
Z160076	Coma	Sc	0.65	13.64	96	-0.23	47	-12.83	5
Z160086	Coma	Pec	0.37	13.18	96	0.76	41	-13.04	5
Z160088	Coma	Sb	1.05	11.12	96	0.20	16	-12.65	5
Z160095	Coma	Sb	0.35	9.50	96	0.72	4	-12.66	5
Z160096N	Coma	Pec	1.37	11.36	96	0.02	39	-12.51	3
Z160098	Coma	Pec	0.77	12.04	96	0.17	22	-12.95	5
Z160102	Coma	Sab	1.14	11.13	96	0.13	6	-12.63	2
Z160106	Coma	Pec	0.59	10.84	96	0.33	20	-12.98	2
Z160108	Coma	Pec	0.56	12.90	96	0.45	37	-13.00	11
Z160121	Coma	Sb	1.64	11.21	96	0.05	21	-12.93	T.W.
Z160127	Coma	Sc	1.21	13.29	96	-0.01	67	-12.53	5
Z160128	Coma	Pec	1.29	13.67	96	-	87	-12.65	5
Z160137	Coma	Sa	1.77	10.57	96	0.00	11	-12.51	2
Z160139	Coma	Pec	1.71	13.26	96	-0.04	51	-12.58	5
Z160141	Coma	Pec	1.61	12.51	96	0.39	30	-13.08	11
Z160148	Iso	Sa	1.99	10.73	80	0.11	7	-12.83	2
Z160151	Iso	Pec	2.48	12.57	83	0.40	28	-12.87	3
Z160152	Iso	Sb	2.36	10.85	75	0.02	17	-12.32	2
Z160156	Prs	Sa	2.91	10.98	97	0.23	10	-12.81	3
Z160168	Iso	Sc	4.19	10.87	100	-0.34	15	-12.50	5
Z160182	Iso	Sab	3.97	11.13	93	0.11	12	-12.72	3
Z160192	Iso	Sb	4.27	10.49	88	-0.12	2	-13.20	5
Z160213	Coma	Pec	0.24	13.07	96	-0.08	57	-12.87	7
Z160252	Coma	Pec	0.18	12.37	96	0.10	37	-12.88	14
Z160257	Coma	Sa	0.27	10.55	96	0.69	6	-12.93	2
Z160260	Coma	Sa	0.30	10.29	96	0.50	11	-12.61	14
Z161040	Iso	Sc	5.42	12.73	97	0.09	21	-13.18	11
Z161052	Iso	Pec	6.15	12.55	94	-0.57	44	-12.67	11
Z161054	Iso	Sa	6.62	12.84	90	-	43	-12.73	11
Z161063	Iso	Sbc	6.83	12.62	95	-0.05	22	-12.89	5
Z161069	Iso	Sb	7.22	11.15	95	-0.30	24	-12.46	7

## Coma/A1367 supercluster. Cont.

Gal	Agg	Type	$\Theta$ Deg.	H mag	Dist. Mpc	$Def_{gas}$	$H_\alpha + [NII]E.W.$ $\text{\AA}$	$LogF(H_\alpha)$ erg cm $^{-2}$ s $^{-1}$	ref
(1)	(2)	(3)	(4)	(5)	(6)	(7)	(8)	(9)	(10)
Z161071	Iso	Pec	7.40	13.22	64	-0.16	48	-12.55	3
Z161073	Iso	Sb	7.55	10.31	97	-0.21	4	-12.83	3

References: (1) Kennicutt & Kent, 1983; (2) Kennicutt, Bothun & Schommer, 1984; (3) Gavazzi, Boselli & Kennicutt, 1991; (4) Romanishin, 1990; (5) Gavazzi et al., 1998; (6) Almoznino & Brosch, 1998; (7) Boselli & Gavazzi, 2002 (8) Moss, Whittle & Pesce, 1998; (9) Heller, Almoznino & Brosch, 1999; (10) Usui, Saito, & Tomita A., 1998; (11) Gavazzi et al. 2002a; (12) Boselli et al., 2002b; (13) Koopmann, Kenney & Joung, 2001; (14) Iglesias et al., 2002; (T.W.) This work.

**Fig. 14.** Newly observed galaxies with substantial  $H\alpha + [NII]$  structure. The NET (ON-OFF) frames are given with grey-scale, with superposed contours of the OFF frames. J2000 celestial coordinates are given.

**Fig. 14.** Continued.

**Fig. 14.** Continued.

This figure "figps\_1.jpg" is available in "jpg" format from:

<http://arxiv.org/ps/astro-ph/0209616v1>

This figure "figps\_2.jpg" is available in "jpg" format from:

<http://arxiv.org/ps/astro-ph/0209616v1>

This figure "figps\_3.jpg" is available in "jpg" format from:

<http://arxiv.org/ps/astro-ph/0209616v1>